IOP Publishing Journal of Optics
J. Opt. 23 (2021) 125701 (12pp) https://doi.org/10.1088/2040-8986/ac2eab

Integral order photonic RF signal processors based on a soliton crystal micro-comb source

Mengxi Tan[1], Xingyuan Xu[8], Jiayang Wu[1], Bill Corcoran[2], Andreas Boes[3], Thach G Nguyen[3], Sai T Chu[4], Brent E Little[5], Roberto Morandotti[6,7], Arnan Mitchell[3] and David J Moss[1,*]

[1] Optical Sciences Centre, Swinburne University of Technology, Hawthorn, VIC 3122, Australia
[2] Department of Electrical and Computer Systems Engineering, Monash University, Clayton 3800, VIC, Australia
[3] ARC Centre of Excellence for Ultrahigh-bandwidth Devices for Optical Systems (CUDOS), RMIT University, Melbourne, VIC 3001, Australia
[4] Department of Physics, City University of Hong Kong, Tat Chee Avenue, Hong Kong, People's Republic of China
[5] Xi'an Institute of Optics and Precision Mechanics of CAS, Xi'an 710119, People's Republic of China
[6] INRS-Énergie, Matériaux et Télécommunications, 1650 Boulevard Lionel-Boulet, Varennes, Québec J3X 1S2, Canada
[7] Also, a visiting Professor with the Institute of Fundamental and Frontier Sciences, University of Electronic Science and Technology of China, Chengdu 610054, People's Republic of China
[8] Electro-Photonics Laboratory, Department of Electrical and Computer System Engineering, Monash University, Clayton 3800, VIC

E-mail: dmoss@swin.edu.au

Received 8 May 2021, revised 28 September 2021
Accepted for publication 11 October 2021
Published 27 October 2021

Abstract

Soliton crystal micro-combs are powerful tools as sources of multiple wavelength channels for radio frequency (RF) signal processing. They offer a compact device footprint, a large number of wavelengths, very high versatility, and wide Nyquist bandwidths. Here, we demonstrate integral order RF signal processing functions based on a soliton crystal micro-comb, including a Hilbert transformer and first, second and third-order differentiators. We compare and contrast the results and the trade-offs involved with varying the comb spacing, and tap design and shaping methods.

Keywords: RF photonics, optical resonators, signal processor

(Some figures may appear in colour only in the online journal)

1. Introduction

Radio frequency (RF) signal processing functions, including the Hilbert transform and differentiation, are building blocks of advanced RF applications such as radar systems, single sideband modulators, measurement systems, speech processing, signal sampling, and communications [1–50]. Although the electronic digital-domain tools that are widely employed enable versatile and flexible signal processing functions, they are subject to the electronic bandwidth bottleneck of analog-to-digital converters [4], and thus face challenges in processing wideband signals.

Photonic microwave and RF systems [1–10] have experienced significant attention over the past 20 years because of their combined ability to achieve very high bandwidths, together with their low loss and very high immunity to electromagnetic interference. Many approaches to photonic RF signal

* Author to whom any correspondence should be addressed.

processing have been proposed that take advantage of the coherence of the RF imprinted optical signals—thereby inducing optical interference. These coherent approaches map the response of optical filters, implemented through optical resonators or nonlinear effects, onto the RF domain [7–12]. As such, the ultimate performance of the RF filters largely depends on the optical filters. State-of-art demonstrations of coherent photonic RF filters include those that use integrated micro-ring resonators (MRRs), with Q factors of >1 million, as well as techniques that employ on-chip (waveguide-based) stimulated Brillouin scattering [13, 14]. Both of these approaches have their unique advantages—the former uses passive devices and so can achieve very low power consumption, while the latter can achieve a much higher frequency selectivity, reaching a 3 dB bandwidth resolution as low as 32 MHz.

Coherent approaches generally focus on narrow-band applications where the frequency range of concern is narrow and the focus is on frequency selectivity, and where the filters are generally band-pass or band-stop in nature. In contrast, incoherent approaches that employ transversal filtering structures can achieve a very diverse range of functions over a much wider frequency range, such as Hilbert transforms and differentiations. The transversal structure originates from the classic digital finite impulse response filter, where the transfer function is achieved by weighting, delaying and summing the input signals. Unlike digital approaches that operate under von-Neumann protocols, photonic implementations achieve the entire process through analog photonics, where the weighting, delaying and summing happens physically at the location of the signals, instead of reading and writing back-and-forth from memory.

To achieve the transversal structure optically, four steps are required. First, the input RF signals are replicated, or multicast, onto multiple wavelengths simultaneously using wavelengths supplied from either multiple single wavelength, or single multiple wavelength, sources. Next, the replicated signals are assigned different weights for each wavelength, and then the composite signal is progressively delayed where each wavelength is incrementally delayed relative to the adjacent. Finally, the weighted replicas are summed together by photodetecting the entire signal. The underpinning principle to this process is to physically achieve multiple parallel channels where each channel carries and processes one replica of the RF signal. In addition to wavelength multiplexing techniques, this can also be accomplished with spatial multiplexing, such using an array of fibre delay lines to spatially achieve the required parallelism. Although this is straightforward to implement, it suffers from severe tradeoffs between the number of channels and overall footprint and cost. Exploiting the wavelength dimension is a much more elegant approach since it makes much better use of the wide optical bandwidth of over the 10 THz that the telecommunications C-band offers, and thus is more compact. However, traditional approaches to generating multiple optical wavelengths have been based on discrete laser arrays [6–10], and these face limitations in terms of a large footprint, relatively high cost, and challenges in terms of accurate control of the wavelength spacing.

Optical frequency combs—equally spaced optical frequency lines—are a powerful approach to implementing incoherent photonic RF filters since they can provide a large number of wavelength channels with equal frequency spacings, and in a compact scheme. Among the many traditional methods of achieving optical frequency combs, electro-optic (EO) techniques have probably experienced the widest use for RF photonics. By simultaneously driving cascaded EO modulators with a high-frequency RF source, a large number of comb lines can be generated, and these have been the basis of many powerful functions [46–50]. However, EO combs are not without challenges. On the one hand, they generally have a small Nyquist zone (half of the frequency spacing), limited by the RF source, but the bulky optical and RF devices are challenging to be monolithically integrated. As such, to address the issues of size, reliability and cost-effectiveness for photonic RF systems, integrated frequency combs are a highly attractive approach.

Integrated Kerr optical frequency combs [51–77], or micro-combs, that originate via optical parametric oscillation in monolithic MRRs, have recently attracted significant attention as an innovative and powerful approach to RF photonics because of their ability to generate many highly coherent multiple wavelength channels in an integrated single chip source. They offer a much higher number of wavelengths than typically is available through EO combs, together with a wide range of comb spacings (free spectral range (FSR)) including ultra-large FSRs, as well as a very small size and low complexity. Micro-combs have enabled many fundamental breakthroughs including ultrahigh capacity communications [78–80], neural networks [81–83], complex quantum state generation [84–91] and much more. In particular, they have proven to be very powerful tools for a wide range of RF applications such as optical true time delays [31], transversal filters [34, 39], signal processors [29, 32], channelizers [38, 45] and others [15, 18, 26–45]. They have greatly expanded the capability and performance of microwave signal processors in many respects, including increased resolution (for coherent systems) together with larger bandwidths (for incoherent systems).

In one of the first reports of using micro-combs for RF signal processing, we demonstrated a Hilbert transformer based on a transversal filter that employed up to 20 taps, or wavelengths [36, 37]. This was based on a 200 GHz FSR spaced micro-comb source that operated in a semi-coherent mode that did not feature solitons. Nonetheless, this provided a low enough noise comb source to enable very attractive performance, achieving a bandwidth of over five octaves in the RF domain. Subsequently [15], we demonstrated 1st, 2nd and 3rd order integral differentiators based on the same 200 GHz source, achieving high RF performance with bandwidths of over 26 GHz, as well as a range of RF spectral filters including bandpass, tunable bandpass and gain equalizing filters [32, 33].

Recently, a powerful category of micro-combs—soliton crystals—has been reported [59, 60, 77]. They feature ultra-low intensity noise states and straightforward generation methods using only adiabatic pump wavelength sweeping. Soliton crystals are unique solutions to the parametric dynamics governed by the Lugiato-Lefever equation. They are tightly packaged solitons circulating along the ring cavity, stabilized by a background wave generated by a mode-crossing. Due to their much higher intra-cavity intensity compared with the single-soliton Dissipative Kerr solitons (DKS) states, thermal effects that typically occur during the transition from chaotic to coherent soliton states are negligible, thus alleviating the need for complex pump sweeping methods.

We have exploited soliton crystal states generated in record low FSR (49 GHz) MRRs, thus generating a record large number of wavelengths, or taps, to achieve a broad array of microwave and RF signal processing functions. These include RF filters [35], true time delays [30], RF integration [43], fractional Hilbert transforms [27], fractional differentiation [42], phase-encoded signal generation [26], arbitrary waveform generation [44], filters realized by bandwidth scaling [39], and RF channelizers [45].

In this work, we further examine transversal photonic RF signal processors that exploit soliton crystal micro-combs. We demonstrate integral order Hilbert transformers as well as 1st, 2nd, and 3rd order integral differentiators and explore in detail the inherent trade-offs between using differently spaced soliton crystal micro-combs and different numbers of tap weights as well as design methods. Our study sheds light on the optimum number of taps, while the experimental results agree well with theory, verifying the feasibility of our approach towards the realization of high-performance photonic RF signal processing with potentially reduced cost, footprint and complexity.

2. Operation principle

The formation of Kerr micro-combs is a fundamentally complex process that is enhanced by a high 3rd order nonlinear material refractive index, low linear loss, low two photon absorption, as well as carefully designed dispersion which generally needs to be anomalous in the spectral region of interest [51–65]. A wide range of material platforms have been used to demonstrate micro-comb generation [58], such as magnesium fluoride, silica glass, doped silica glass, or Hydex [66–77], and silicon nitride [53–65]. The MRRs that are the basis to generate the Kerr soliton crystal micro-combs used in this work are shown in figure 1(a). They were fabricated in Hydex glass, a doped silica glass, high refractive index platform, together with Complementary metal-oxide-semiconductor (CMOS) compatible fabrication processes. This platform displays very low linear and nonlinear optical loss, and so very high Q factor MRRs can be produced that feature narrow resonance linewidths, corresponding to Q factors as high as 1.5×10^6. Further, we were able to achieve oscillation in MRRs that had radii as large as $\sim$592 μm, yielding a very low FSR of $\sim$0.393 nm, corresponding to $\sim$48.9 GHz (figure 1(b)) [54, 55]. For the fabrication process, first Hydex glass was deposited featuring a high-index ($n = \sim$1.7 at 1550 nm). The deposition process was low temperature plasma-enhanced chemical vapour deposition, which was combined with lithography methods pattern to the waveguides, which were based on deep UV stepper mask photolithography. Etching was performed via reactive ion etching, and the last step consisted of deposition of the upper cladding layer. Our devices tend to use a vertical coupling design with a ring resonator core to bus waveguide core gap typically being about 200 nm. This approach can control the gap much more accurately than via lithographic methods since it is determined by film growth. The advantages of the Hydex platform in terms of Kerr optical micro-combs include a very low linear optical loss of typically $\sim$0.06 dB cm^{-1}, together with a moderately large Kerr nonlinearity of about $\sim$233 W^{-1} km^{-1} and most importantly, a vanishing two photon absorption even up to extremely high intensities of $\sim$25 GW cm^{-2} [66–78]. The devices were integrated with on-chip mode converters which allowed them to be packaged with fibre pigtails, resulting in a very low insertion loss for the through-port of 0.5 dB/facet.

To generate soliton crystal micro-combs, we amplified the pump power up to 30.5 dBm. When the detuning between the pump wavelength and the unpumped resonance wavelength decreased so that the power in the MRR reached a threshold, modulation instability (MI) gain driven oscillation occurred.

This initially generated primary combs with a wavelength spacing governed by the peak wavelength of the MI gain, which is a function of both the dispersion and power inside the MRR. As the detuning decreased further, distinctive optical spectra were finally observed (figure 1(d)) that were indicative of what has been seen from the spectral interference between tightly packed solitons in a cavity—so-called 'soliton crystals' [59, 60]. A second power step jump in the measured intra-cavity power was observed at this point, where the soliton crystal spectra appeared. For microwave and RF applications, particularly with transversal filter structures, we have found that it is not absolutely necessary to achieve complete coherence of the comb lines, or that any specific state is needed such as either single soliton states (DKS) or soliton crystals, in order to achieve high system performance. The only important criterion is to avoid the completely chaotic regime [58] where the RF noise is extremely high. Notwithstanding this, the coherent states still yield the best overall performance and indeed, the soliton crystal states provide the lowest noise states of all the micro-combs that we have employed. As a result, we have focused on these states as the basis for microwave oscillators with extremely low phase-noise [28]. This is an important point since there exists a much wider range of low RF noise coherent states that are more easily achievable than any specific state related to pure solitons [58].

Figure 2 illustrates the conceptual diagram of the transversal structure. A given set of weighted and delayed copies of the input RF signal are multicast onto the comb wavelengths in the optical domain and subsequently summed after photodetection. Generally, the transfer function of a transversal signal processor is given by

$$H(\omega) = \sum_{n=0}^{N-1} a_n \mathrm{e}^{-j\omega nT} \qquad (1)$$

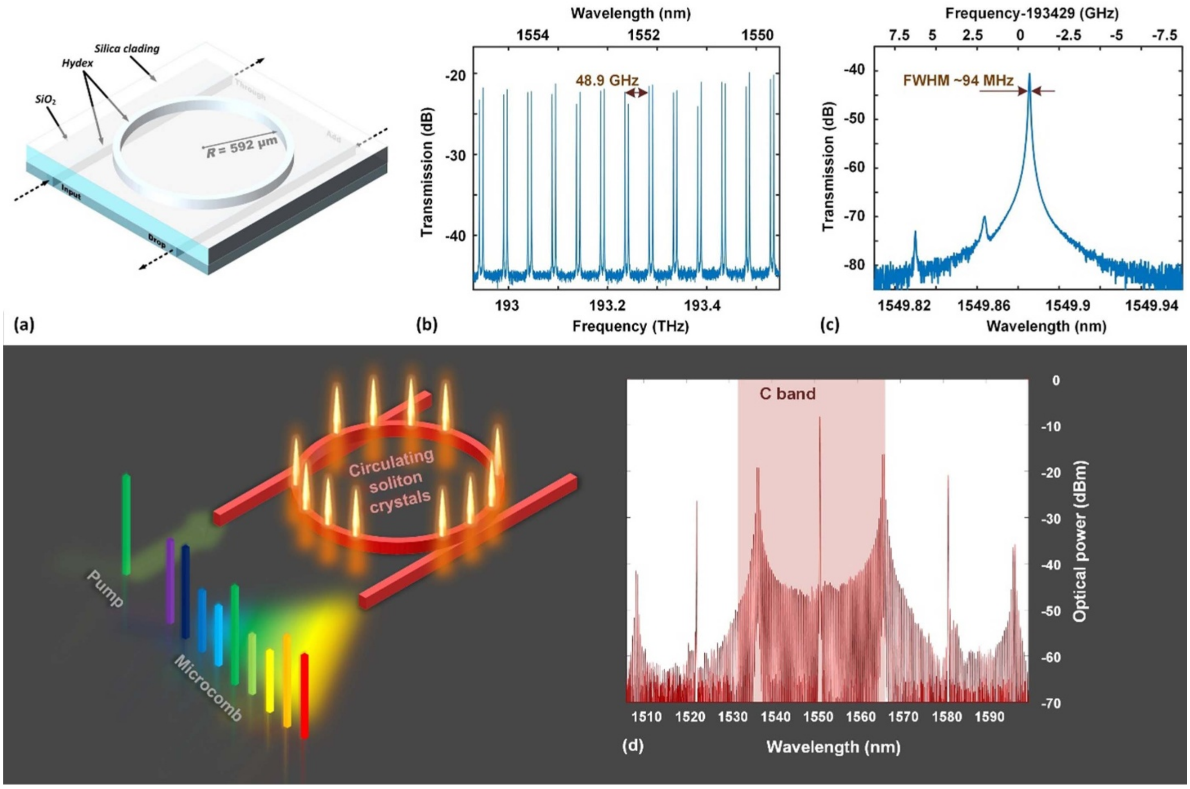

Figure 1. (a) Schematic of the micro-ring resonator. (b) Drop-port transmission spectrum of the integrated MRR with a span of 5 nm, showing an optical free spectral range of 48.9 GHz. (c) A resonance at 193.429 THz with a full width at half maximum (FWHM) of $\sim$94 MHz, corresponding to a quality factor of $\sim 2 \times 10^6$. (d) (Bottom) Schematic illustration of the integrated MRR for generating the Kerr frequency comb and the optical spectrum of the generated soliton crystal combs with a 100 nm span.

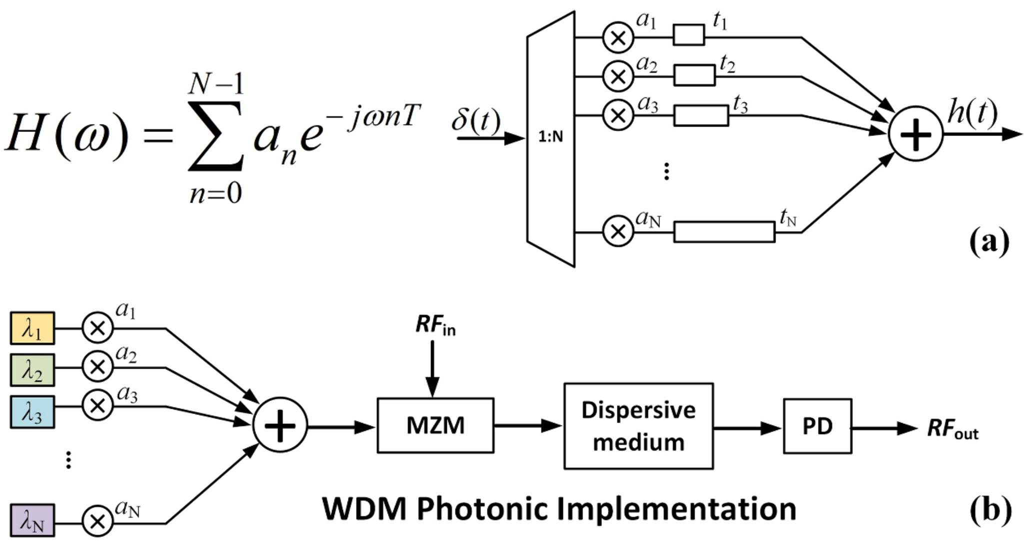

Figure 2. Conceptual diagram of the transversal structure. (a) $H(\omega)$ is the transfer function of the transversal structure, where ω denotes the angular frequency, N equals the number of taps, α_{n} is the tap weight of the n_{th} tap, and T is the corresponding delays. (b) Experimental realization of the transfer function. Multiwavelength comb sources with different wavelengths provide different delay taps—each wavelength has a different delay generated by the dispersive medium. The summation function is performed by photodetection of the composite signal.

where N is the number of taps, ω the RF angular frequency, T the time delay between adjacent taps, and a_n the tap coefficient of the nth tap, which is the discrete impulse response of the transfer function $F(\omega)$ of the signal processor. The discrete impulse response a_n can be calculated by performing the inverse Fourier transform of the transfer function $F(\omega)$ of the signal processor [11]. The FSR of the RF signal processor is determined by T, since $\mathrm{FSR}_{\mathrm{RF}} = 1/T$. As the multi-wavelength

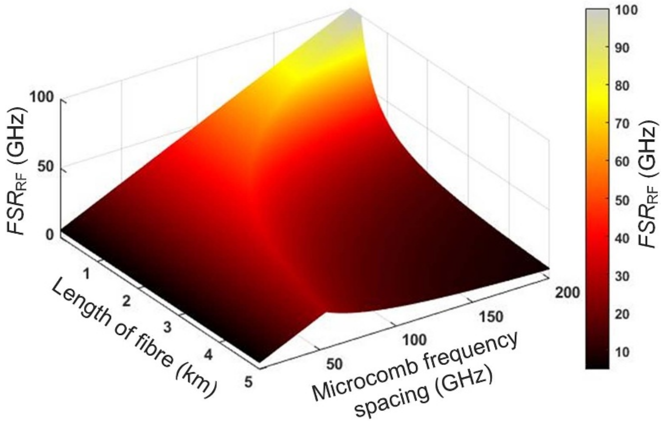

Figure 3. Free spectral range of the RF transversal signal processor according to the length of fibre and comb spacing. Here we used single mode fibre with the second order dispersion coefficient of $\beta = \sim$17.4 ps nm^{-1} km^{-1} at 1550 nm for the calculation of $\mathrm{FSR_{RF}}$.

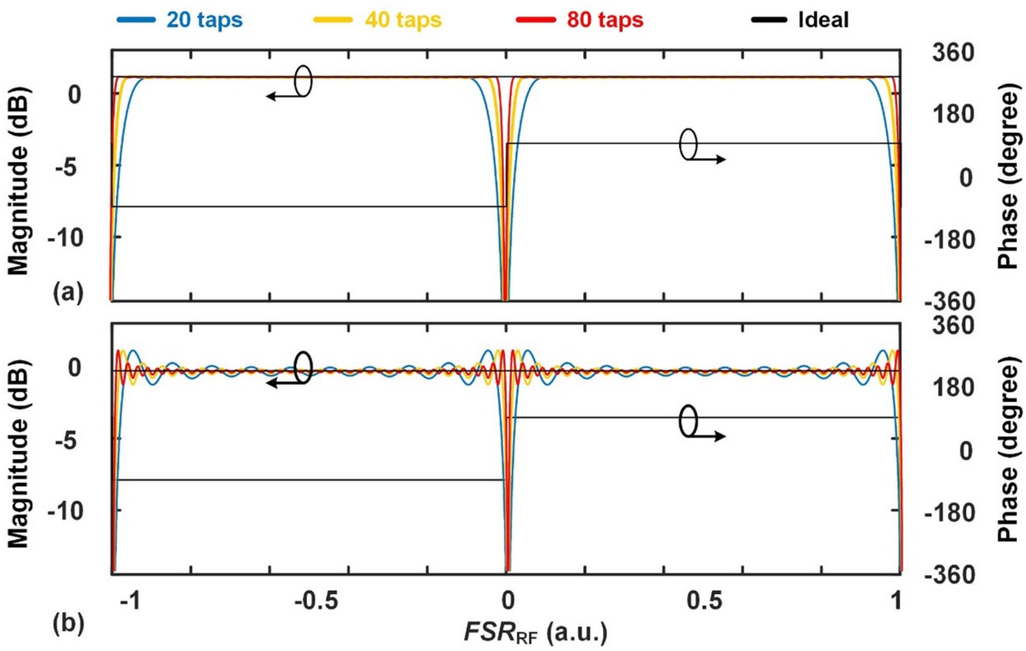

Figure 4. Theoretical and simulated RF magnitude according to the number of taps and ideal phase response of a Hilbert transformer with 90° phase shift. (a) With a hamming window applied. (b) Without window method applied.

optical comb is transmitted through the dispersive medium, the time delay can be expressed as

$$T = D \times L \times \Delta\lambda \quad (2)$$

where D is the dispersion coefficient, L the length of the dispersive medium, and $\Delta\lambda$ is the wavelength spacing of the soliton crystal micro-comb (figure 1) which indicates the potentially broad bandwidth RF signal that the system can process. Figure 3 shows the relationship between the wavelength spacing of the comb, the total delay of the fibre, and the resulting RF FSR, or essentially the Nyquist zone. The operation bandwidth can be readily varied by changing the time delay via a number of means, such as using different delay components. The largest operational bandwidth of the transversal signal processor is given by the Nyquist frequency which is half of the comb spacing. Thus, employing a comb shaping method to achieve a larger comb spacing could enlarge the maximum operational bandwidth. However, this comes with the tradeoff that it yields fewer taps, or wavelengths, over the wavelength range of interest, which in our case is the telecommunications C-band. Hence, the number of comb lines/taps as well as the comb spacing, are both key parameters that determine the performance of the signal processor. We investigate this tradeoff in this paper.

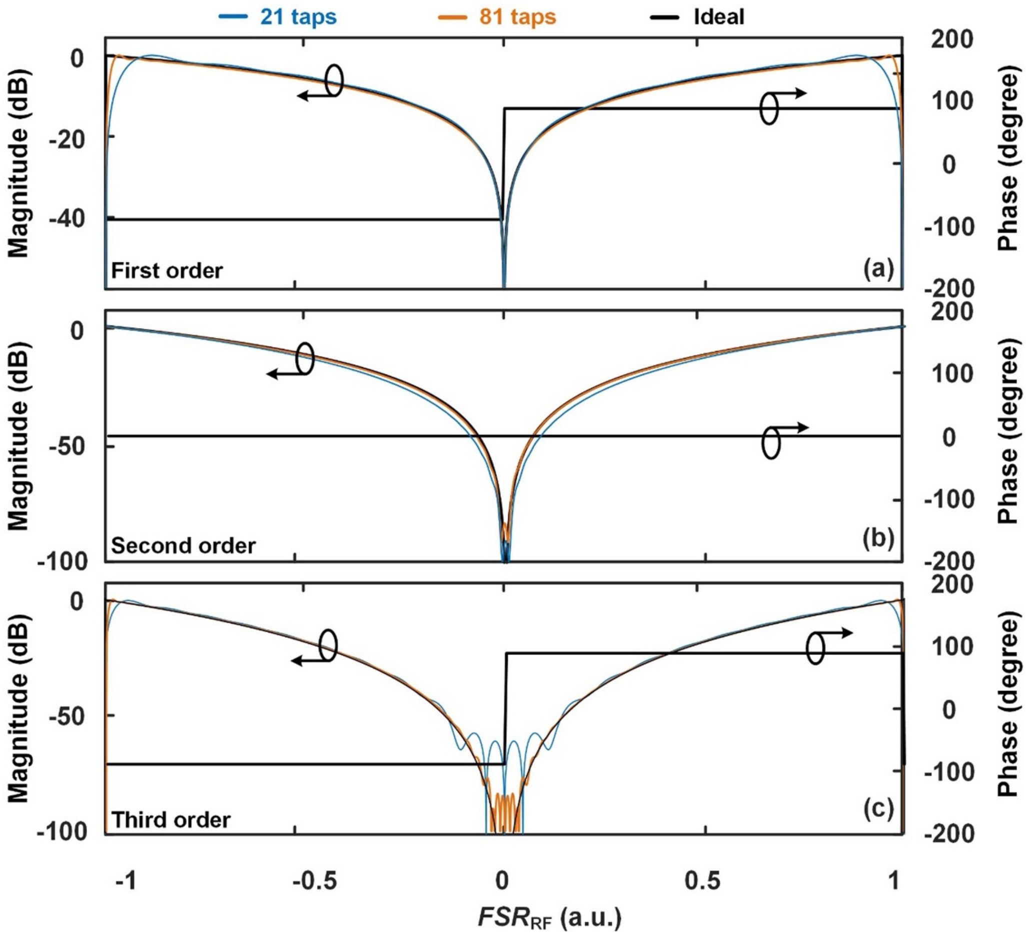

Figure 5. Theoretical and simulated RF magnitude according to the number of taps and ideal phase response of (a) first-order differentiator. (b) Second-order differentiator. (c) Third-order differentiator.

Figures 4 and 5 show the theoretically calculated performance of the Hilbert transformer with a 90° phase shift together with the 1st, 2nd and 3rd order integral differentiators in terms of their filter amplitude response, as a function of the number of taps. Note that a Hamming window [11] is applied in figure 4(a), in order to suppress the sidelobes of the Hilbert transformer. To implement the temporal differentiator and Hilbert transformer, tap coefficients in equation (1) were calculated based on the Remez algorithm [92].

3. Experiment

Figure 6 shows the experimental setup of the transversal filter signal processor based on a soliton crystal micro-comb. It consists mainly of two parts—comb generation and flattening followed by the transversal structure. In the first part, the generated soliton crystal micro-comb was spectrally shaped with two WaveShapers to enable a better signal-to-noise ratio as well as a higher shaping accuracy. The first WaveShaper (WS1) was used to equalize, or flatten, the comb spectrum from the orignally generated scallop-shaped pattern that is typical of soliton crystal micro-combs. In the second stage of the system, these equalized comb lines were all simultaneously modulated by the RF input signal with an EO modulator, which effectively multicast the RF signal onto all wavelength channels to yield identical copies. The RF replicas were then transmitted through a spool of standard SMF ($\beta = \sim 17.4$ ps nm^{-1} km^{-1}) to obtain a progressive time delay between the adjacent wavelengths. Next, the second WaveShaper (WS2) equalized and weighted the power of the comb lines according to the designed tap coefficients. To increase the accuracy, we adopted a real-time feedback control path to read and shape the power of the comb lines accurately. Finally, the weighted and delayed taps were combined and converted back into the RF domain via a high-speed balanced photodetector (Finisar, 43 GHz bandwidth).

Figure 7 shows the experimental results for the Hilbert transformer with a 90° phase shift. The shaped optical combs are shown in figures 7(a), (e) and (i). A good match between the measured comb lines' power (blue lines for positive, black lines for negative taps) with the theoretically calculated design tap weights (red dots) was achieved, indicating that the micro-comb wavelengths were successfully weighted. Note that we

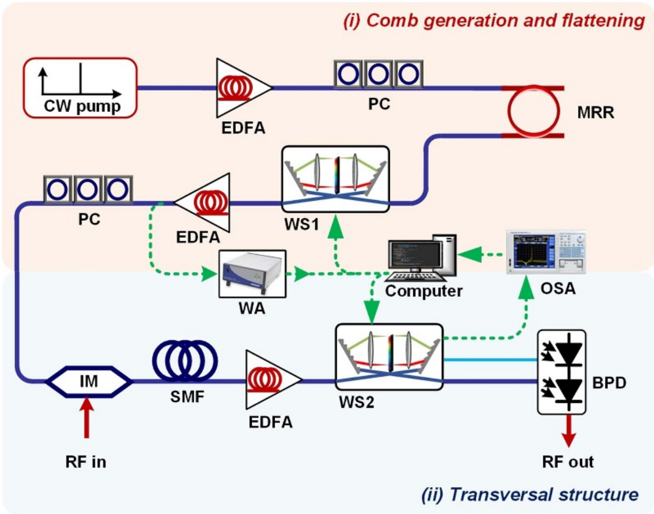

Figure 6. Experimental set up of RF signal processor based on soliton crystal micro-comb source. CW: continuously wave. EDFA: erbium-doped fibre amplifier. PC: polarization controller. WS: WaveShaper. IM: intensity modulator. SMF: single mode fibre. BPD: balanced photodetector. WA: wave analyzer. OSA: optical spectral analyzer.

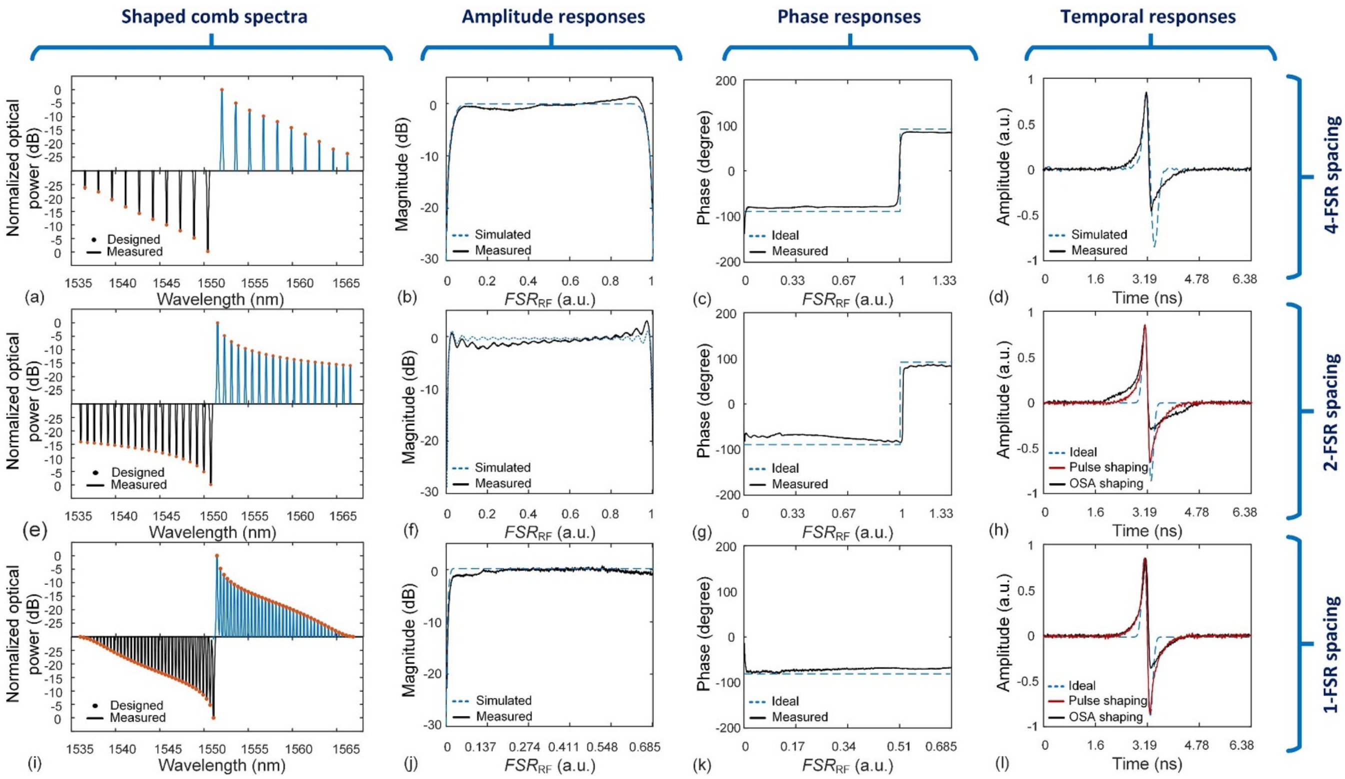

Figure 7. Simulated and measured 90° Hilbert transformer with varying comb spacing. (a), (e) and (i) Shaped optical spectral. (b), (f) and (j) Amplitude responses (the |S21| responses measured by a Vector Network Analyzer). (c), (g) and (k) Phase responses. (d), (h) and (l) Temporal responses measured with a Gaussian pulse input.

applied a Hamming window [11] for single-FSR (49 GHz) and 4-FSR (196 GHz) comb spacings when designing the tap coefficients. One can see that with a Hamming window applied, the deviation of the amplitude response from the theoretical results can be improved. Figures 7(b), (f) and (j) show the theoretical and experimentally measured amplitude response of the Hilbert transformer using a variety of different combs having different spacings, including single-FSR, 2-FSR, and 4-FSR comb spacings, respectively, while the phase responses are shown in figures 7(c), (g) and (k). We see that all 3 results show behaviour close the expected response of an ideal Hilbert transform. The system demonstration for the

Table 1. Performance of our transversal signal processors.

Type	Number of taps	Wavelength spacing	Frequency spacing (GHz)	Nyquist zone (GHz)	Octave	Temporal pulse RMSE	
						OSA shaping	Pulse shaping
Hilbert transformer	20	4-FSR	196	98	>4.5	∼0.0957	/
Hilbert transformer	40	2-FSR	98	49	>6	∼0.1065	∼0.0845
Hilbert transformer	80	Single-FSR	49	24.5	/	∼0.1330	∼0.0782
Differentiator—1st order	21	4-FSR	196	98	/	∼0.0838	/
Differentiator—2nd order	21	4-FSR	196	98	/	∼0.0570	/
Differentiator—3rd order	21	4-FSR	196	98	/	∼0.1718	/
Differentiator—1st order	81	Single-FSR	49	24.5	/	∼0.1111	/
Differentiator—2nd order	81	Single-FSR	49	24.5	/	∼0.1139	∼0.0620
Differentiator—3rd order	81	Single-FSR	49	24.5	/	∼0.1590	/

Hilbert transform using real-time signals consisting of Gaussian input pulses produced by an arbitrary waveform generator (KEYSIGHT M9505A) is shown in figures 7(d), (h) and (l) (black solid curves), recorded by a real-time high-speed oscilloscope (KEYSIGHT DSOZ504). To facilitate a comparison, we also show the response of an ideal Hilbert transformer in figures 7(d), (h) and (l) (blue dashed curves). For the Hilbert transformer with single-FSR, 2-FSR, and 4-FSR comb spacings, the root-mean-square errors (RMSEs) between the theoretical and experimentally measured curves were ∼0.133, ∼0.1065, and ∼0.0957. The performance parameters are listed in table 1.

Figure 8 shows the experimental results for the differentiators with increasing integral orders of 1, 2, and 3. The shaped optical spectra in figures 8(a), (e), (i), (m), (q) and (u) show good agreement between the theoretical tap weights and measured comb lines' power. Figures 8(b), (f), (j), (n), (r) and (v) show measured and simulated amplitude responses of the differentiators. The corresponding phase response is depicted in figures 8(c), (g), (k), (o), (s) and (w) where it can be seen that all (b), (f), (j), (n), (r) and (v) show measured and simulated amplit integral differentiators agree well with the theory.

Here, we use the WaveShaper to programmably shape the combs to simulate MRRs with different FSRs. By artificially adjusting the comb spacing, we effectively obtain a variable operation bandwidth for the differentiator, which is advantageous for the diverse requirements of different applications. Here, we normalised the FSR of the RF response to have the unique operational bandwidth for comparing the performance of different processing functions in the same scales. For the 1st, 2nd, and 3rd order differentiators with a single-FSR (49 GHz) spacing, the calculated RMSEs between the measured and ideal curves are ∼0.1111, ∼0.1139, ∼0.1590, respectively. For the 1st, 2nd, and 3rd order differentiators with a 4-FSR (196 GHz) spacing, the calculated RMSEs between the measured and ideal curves are ∼0.0838, ∼0.0570, ∼0.1718, respectively. Note that there is some observed difference in the time-domain between the positive and negative amplitude and phase responses to the Gaussian input pulse which leads to a discrepancy with the ideal response. This is due to a combination of effects including the residual imbalance of the two ports of the balanced photodetector.

In order to reduce the errors mentioned above, for both the Hilbert transformer and the differentiator, we developed a more accurate comb shaping approach, where the error signal of the feedback loop was generated directly by the measured impulse response, instead of the optical power of the comb lines. We then performed the Hilbert transform and differentiation with the same transversal structure as the previous measurements, the results of which are shown in figures 7(h), (I) and 8(t). One can see that the imbalance of the response in the time domain has been compensated, and the RMSE of time-domain shown in table 1 has significantly improved. While this was the main source of error, the remaining discrepancy between theory and experiment in figures 7 and 8 arises from modulation chirp and third order dispersion in the fibre, which created distortion. In principle these can also be compensated for, and this will be addressed in future work.

Also note that the fact that the soliton crystal micro-comb was able to supply a larger number of comb lines, in our case up to 81 for the 1-FSR spaced comb, resulted in a much higher performance in terms of the spanned number of octaves in the RF domain as well as the RMSE, etc. On the other hand, the disadvantage is that single FSR spaced comb yields a lower operational bandwidth, being limited to approximately the Nyquist zone, which in that case is 25 GHz. The 2-FSR spacing and 4-FSR spaced system, on the other hand, can operate at RF frequencies that are well beyond that of traditional electronic microwave technologies. Therefore our shaping method gives the flexibility for us to achieve the required system.

Finally, figure 9 shows the 3 dB bandwidth of the Hilbert transformer versus the number of taps, for both theoretically calculated and experimentally measured results. As seen in figure 9, the theoretical 3 dB bandwidth increases

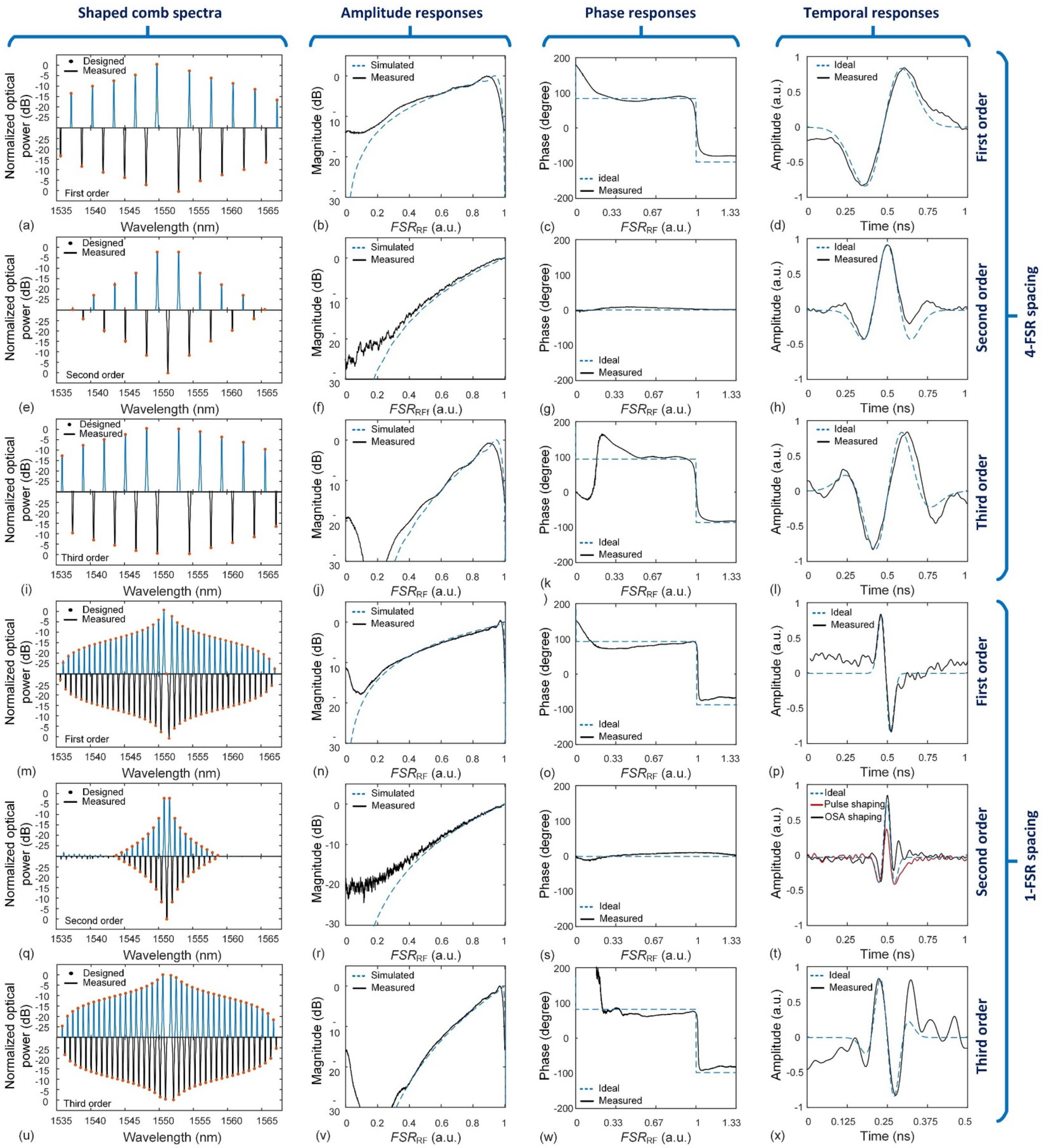

Figure 8. Simulated and measured first- to third-order differentiators with different comb spacing (single-FSR and 4-FSR). (a), (e), (i), (m), (q) and (u) Shaped optical spectral. (b), (f), (j), (n), (r) and (v) Amplitude responses. (c), (g), (k), (o), (s) and (w) Phase responses. (d), (h), (l), (p), (t) and (x) Temporal responses measured with a Gaussian pulse input.

rapidly with the number of taps but begins to saturate beyond 40 taps, meaning that there is limited benefit in including more taps. We note that we have previously shown a similar curve looking at the bandwidth dependence on the number of taps for a fractional Hilbert transformer in figure 5(c) of [27], which showed good agreement between experiment and theory. In figure 9 we only show two measured points—while we did have data for 80 taps, the bandwidth was larger than what we could experimentally measure.

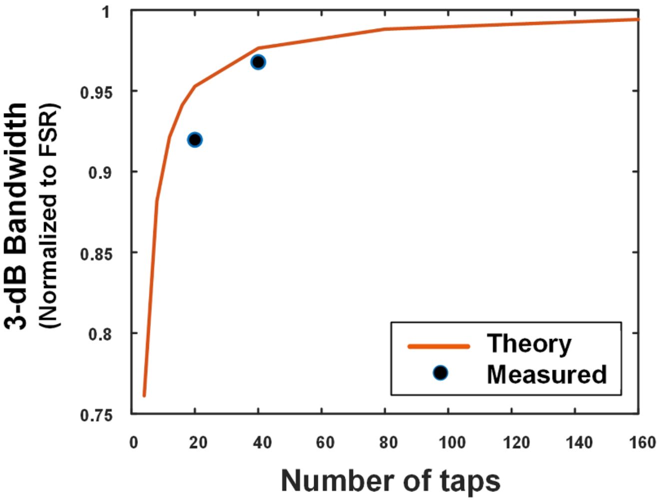

Figure 9. Simulated and experimental results of 3 dB bandwidth with different numbers of taps for a Hilbert transformer with 90° phase shift. The 3 dB bandwidth is expressed as a relative fraction of the RF FSR.

4. Conclusion

We demonstrate record performance and versatility for soliton crystal micro-comb-based RF signal processing functions by varying the wavelength spacing and employing different tap designs and shaping methods. Our experimentally measured system performance agrees well with the theory, thus verifying that our soliton crystal micro-comb-based signal processor is a successful and attractive approach for achieving RF signal processors that feature broad operation bandwidths, a high degree of reconfigurebility, and potentially also reduced cost and footprint.

Data availability statement

The data that support the findings of this study are available upon reasonable request from the authors.

Acknowledgments

This work was supported by the Australian Research Council Discovery Projects Program (No. DP150104327). RM acknowledges support by the Natural Sciences and Engineering Research Council of Canada (NSERC) through the Strategic, Discovery and Acceleration Grants Schemes, and by the Canada Research Chair Program. Brent E Little was supported by the Strategic Priority Research Program of the Chinese Academy of Sciences, Grant No. XDB24030000.

ORCID iDs

Xingyuan Xu https://orcid.org/0000-0002-8190-4700
Andreas Boes https://orcid.org/0000-0001-8443-3396
David J Moss https://orcid.org/0000-0001-5195-1744

References

[1] Capmany J and Novak D 2007 Microwave photonics combines two worlds *Nat. Photon.* **1** 319–30
[2] Yao J P 2009 Microwave photonics *J. Lightwave Technol.* **27** 314–35
[3] Marpaung D, Yao J and Capmany J 2019 Integrated microwave photonics *Nat. Photon.* **13** 80–90
[4] Azaña J 2010 Ultrafast analog all-optical signal processors based on fiber-grating devices *IEEE Photonics J.* **2** 359–86
[5] Capmany J, Ortega B and Pastor D 2006 A tutorial on microwave photonic filters *J. Lightwave Technol.* **24** 201–29
[6] Supradeepa V R, Long C M, Wu R, Ferdous F, Hamidi E, Leaird D E and Weiner A M 2012 Comb-based radiofrequency photonic filters with rapid tunability and high selectivity *Nat. Photon.* **6** 186–94
[7] Malacarne A, Ashrafi R, Li M, LaRochelle S, Yao J and Azaña J 2012 Single-shot photonic time-intensity integration based on a time-spectrum convolution system *Opt. Lett.* **37** 1355–7
[8] Torres-Company V and Weiner A M 2014 Optical frequency comb technology for ultra-broadband radio-frequency photonics *Laser Photonics Rev.* **8** 368–93
[9] Jiang Z, Huang C B, Leaird D E and Weiner A M 2007 Optical arbitrary waveform processing of more than 100 spectral comb lines *Nat. Photon.* **1** 463–7
[10] Minasian R A, Chan E H W and Yi X 2013 Microwave photonic signal processing *Opt. Express* **21** 22918–36
[11] Bancroft J C and Geiger H D 1997 Analysis and design of filters for differentiation *CREWES Res. Rep.* **9** 21–13
[12] Liu Y, Yu Y, Yuan S X, Xu X B and Zhang X L 2016 Tunable megahertz bandwidth microwave photonic notch filter based on a silica microsphere cavity *Opt. Lett.* **41** 5078–81
[13] Marpaung D, Morrison B, Pagani M, Pant R, Choi D Y, Luther-Davies B, Madden S J and Eggleton B J 2015 Low-power, chip-based stimulated Brillouin scattering microwave photonic filter with ultrahigh selectivity *Optica* **2** 76–83
[14] Choudhary A, Morrison B, Aryanfar I, Shahnia S, Pagani M, Liu Y, Vu K, Madden S, Marpaung D and Eggleton B J 2017 Advanced integrated microwave signal processing with giant on-chip Brillouin gain *J. Lightwave Technol.* **35** 846–54
[15] Xu X, Wu J, Shoeiby M, Nguyen T G, Chu S T, Little B E, Morandotti R, Mitchell A and Moss D J 2017 Reconfigurable broadband microwave photonic intensity differentiator based on an integrated optical frequency comb source *APL Photonics* **2** 096104
[16] Zhu X Q, Chen F Y, Peng H F and Chen Z Y 2017 Novel programmable microwave photonic filter with arbitrary filtering shape and linear phase *Opt. Express* **25** 9232–43
[17] Jiang F, Yu Y, Tang H T, Xu L and Zhang X L 2016 Tunable bandpass microwave photonic filter with ultrahigh stopband attenuation and skirt selectivity *Opt. Express* **24** 18655–63
[18] Wu J, Xu X, Nguyen T G, Chu S T, Little B E, Morandotti R, Mitchell A and Moss D J 2018 RF photonics: an optical microcombs' perspective *IEEE J. Sel. Top. Quantum Electron.* **24** 6101020
[19] Hamidi E, Leaird D E and Weiner A M 2010 Tunable programmable microwave photonic filters based on an optical frequency comb *IEEE J. Microw. Theory* **58** 3269–78
[20] Zhu Z J, Chi H, Jin T, Zheng S L, Jin X F and Zhang X M 2017 All-positive-coefficient microwave photonic filter with rectangular response *Opt. Lett.* **42** 3012–5
[21] Mansoori S and Mitchell A 2004 RF transversal filter using an AOTF *IEEE Photonics Technol. Lett.* **16** 879–81
[22] Leng J S, Zhang W and Williams J A R 2004 Optimization of superstructured fiber Bragg gratings for microwave

photonic filters response *IEEE Photonics Technol. Lett.* **16** 1736–8

[23] Delgado-Pinar M, Mora J, Diez A, Andres M V, Ortega B and Capmany J 2005 Tunable and reconfigurable microwave filter by use of a Bragg-grating-based acousto-optic superlattice modulator *Opt. Lett.* **30** 8–10

[24] Yu G, Zhang W and Williams J A R 2000 High-performance microwave transversal filter using fiber Bragg grating arrays *IEEE Photonics Technol. Lett.* **12** 1183–5

[25] Hunter D B, Minasian R A and Krug P A 1995 Tunable optical transversal filter based on chirped gratings *Electron. Lett.* **31** 2205–7

[26] Xu X *et al* 2020 Photonic RF phase-encoded signal generation with a microcomb source *J. Lightwave Technol.* **38** 1722–7

[27] Tan M *et al* 2019 Microwave and RF photonic fractional Hilbert transformer based on a 50GHz Kerr micro-comb *J. Lightwave Technol.* **37** 6097–104

[28] Xu X, Wu J, Tan M, Nguyen T G, Chu S T, Little B E, Morandotti R, Mitchell A and Moss D J 2020 Broadband microwave frequency conversion based on an integrated optical micro-comb source *J. Lightwave Technol.* **38** 332–8

[29] Xu X, Tan M, Wu J, Morandotti R, Mitchell A and Moss D J 2019 Microcomb-based photonic RF signal processing *IEEE Photonics Technol. Lett.* **31** 1854–7

[30] Xu X, Wu J, Nguyen T G, Moein T, Chu S T, Little B E, Morandotti R, Mitchell A and Moss D J 2018 Photonic microwave true time delays for phased array antennas using a 49 GHz FSR integrated optical micro-comb source *Photonics Res.* **6** B30–B36

[31] Xue X, Xuan Y, Bao C, Li S, Zheng X, Zhou B, Qi M and Weiner A M 2018 Microcomb-based true-time-delay network for microwave beamforming with arbitrary beam pattern control *J. Lightwave Technol.* **36** 2312–21

[32] Xu X, Wu J, Nguyen T G, Shoeiby M, Chu S T, Little B E, Morandotti R, Mitchell A and Moss D J 2018 Advanced RF and microwave functions based on an integrated optical frequency comb source *Opt. Express* **26** 2569–83

[33] Tan M, Xu X, Wu J, Morandotti R, Mitchell A and Moss D J 2020 Photonic RF and microwave filters based on 49GHz and 200GHz Kerr microcombs *Opt. Commun.* **465** 125563

[34] Xue X, Xuan Y, Kim H-J, Wang J, Leaird D E, Qi M and Weiner A M 2014 Programmable single-bandpass photonic RF filter based on a Kerr comb from a microring *J. Lightwave Technol.* **32** 3557–65

[35] Xu X, Tan M, Wu J, Nguyen T G, Chu S T, Little B E, Morandotti R, Mitchell A and Moss D J 2019 Advanced adaptive photonic RF filters with 80 taps based on an integrated optical micro-comb source *J. Lightwave Technol.* **37** 1288–95

[36] Nguyen T G, Shoeiby M, Chu S T, Little B E, Morandotti R, Mitchell A and Moss D J 2015 Integrated frequency comb source-based Hilbert transformer for wideband microwave photonic phase analysis *Opt. Express* **23** 22087–97

[37] Nguyen T G, Shoeiby M, Chu S T, Little B E, Morandotti R, Mitchell A and Moss D J Quadrature hybrid RF photonic coupler using an integrated frequency comb source *Paper IT2B.4, OSA Advanced Photonics Congress, Topical Meeting on Integrated Photonics Research (Boston, June 2015)* (https://doi.org/10.1364/IPRSN.2015.IT2B.4)

[38] Xu X, Wu J, Nguyen T G, Chu S T, Little B E, Morandotti R, Mitchell A and Moss D J 2018 Broadband RF channelizer based on an integrated optical frequency Kerr comb source *J. Lightwave Technol.* **36** 4519–26

[39] Xu X, Tan M, Wu J, Nguyen T G, Chu S T, Little B E, Morandotti R, Mitchell A and Moss D J 2019 High performance RF filters via bandwidth scaling with Kerr micro-combs *APL Photonics* **4** 026102

[40] Xu X, Wu J, Jia L, Tan M, Nguyen T G, Chu S T, Little B E, Morandotti R, Mitchell A and Moss D J 2018 Continuously tunable orthogonally polarized RF optical single sideband generator based on micro-ring resonators *J. Opt.* **20** 115701

[41] Xu X, Wu J, Tan M, Nguyen T G, Chu S T, Little B E, Morandotti R, Mitchell A and Moss D J 2018 Orthogonally polarized RF optical single sideband generation and dual-channel equalization based on an integrated microring resonator *J. Lightwave Technol.* **36** 4808–18

[42] Tan M *et al* 2020 RF and microwave fractional differentiator based on photonics *IEEE Trans. Circuits Syst.* II **37** 2767–71

[43] Xu X *et al* 2020 Photonic RF and microwave integrator with soliton crystal microcombs *IEEE Trans. Circuits Syst.* **67** 3582–6

[44] Tan M *et al* 2020 Photonic RF arbitrary waveform generator based on a soliton crystal micro-comb source *J. Lightwave Technol.* **38** 6221–6

[45] Xu X, Tan M, Wu J, Boes A, Nguyen T G, Chu S T, Little B E, Morandotti R, Mitchell A and Moss D J 2020 Broadband photonic radio frequency channelizer with 90 channels based on a soliton crystal microcomb *J. Lightwave Technol.* **38** 5116–21

[46] Metcalf A J, Kim H-J, Leaird D E, Jaramillo-Villegas J A, McKinzie K A, Lal V, Hosseini A, Hoefler G E, Kish F and Weiner A M 2016 Integrated line-by-line optical pulse shaper for high-fidelity and rapidly reconfigurable RF-filtering *Opt. Express* **24** 23925–40

[47] Wu R, Supradeepa V R, Long C M, Leaird D E and Weiner A M 2010 Generation of very flat optical frequency combs from continuous-wave lasers using cascaded intensity and phase modulators driven by tailored radio frequency waveforms *Opt. Lett.* **35** 3234–6

[48] Li W Z and Yao J P 2009 Optical frequency comb generation based on repeated frequency shifting using two Mach-Zehnder modulators and an asymmetric Mach-Zehnder interferometer *Opt. Express* **17** 23712–8

[49] Chen C H, He C, Zhu D, Guo R H, Zhang F Z and Pan S L 2013 Generation of a flat optical frequency comb based on a cascaded polarization modulator and phase modulator *Opt. Lett.* **38** 3137–9

[50] Saitoh T, Kourogi M and Ohtsu M 1996 An optical frequency synthesizer using a waveguide-type optical frequency comb generator at 1.5-µm wavelength *IEEE Photonics Technol. Lett.* **8** 1543–5

[51] Del'haye P, Schliesser A, Arcizet O, Wilken T, Holzwarth R and Kippenberg T J 2007 Optical frequency comb generation from a monolithic micro-resonator *Nature* **450** 1214–7

[52] Liang W, Eliyahu D, Ilchenko V S, Savchenkov A A, Matsko A B, Seidel D and Maleki L 2015 High spectral purity Kerr frequency comb radio frequency photonic oscillator *Nat. Commun.* **6** 7957

[53] Levy J S, Gondarenko A, Foster M A, Turner-Foster A C, Gaeta A L and Lipson M 2010 CMOS-compatible multiple-wavelength oscillator for on-chip optical interconnects *Nat. Photon.* **4** 37–40

[54] Razzari L, Duchesne D, Ferrera M, Morandotti R, Chu S, Little B E and Moss D J 2010 CMOS-compatible integrated optical hyper-parametric oscillator *Nat. Photon.* **4** 41–45

[55] Moss D J, Morandotti R, Gaeta A L and Lipson M 2013 New CMOS-compatible platforms based on silicon nitride and Hydex for nonlinear optics *Nat. Photon.* **7** 597–607

[56] Kippenberg T J, Gaeta A L, Lipson M and Gorodetsky M L 2018 Dissipative Kerr solitons in optical microresonators *Science* **361** eaan8083

[57] Gaeta A L, Lipson M and Kippenberg T J 2019 Photonic-chip-based frequency combs *Nat. Photon.* **13** 158–69

[58] Pasquazi A *et al* 2018 Micro-combs: a novel generation of optical sources *Phys. Rev.* **729** 1–81

[59] Cole D C, Lamb E S, Del'Haye P, Diddams S A and Papp S B 2017 Soliton crystals in Kerr resonators *Nat. Photon.* **11** 671–6
[60] Karpov M, Pfeiffer M H P, Guo H, Weng W, Liu J and Kippenberg T J 2019 Dynamics of soliton crystals in optical microresonators *Nat. Phys.* **15** 1071–7
[61] Xue X, Xuan Y, Liu Y, Wang P-H, Chen S, Wang J, Leaird D E, Qi M and Weiner A M 2015 Mode-locked dark pulse Kerr combs in normal-dispersion microresonators *Nat. Photon.* **9** 594
[62] Bao H *et al* 2019 Laser cavity-soliton microcombs *Nat. Photon.* **13** 384–9
[63] Xue X, Zheng X and Zhou B 2019 Super-efficient temporal solitons in mutually coupled optical cavities *Nat. Photon.* **13** 616–22
[64] Zhou H, Geng Y, Cui W, Huang S-W, Zhou Q, Qiu K and Wei Wong C 2019 Soliton bursts and deterministic dissipative Kerr soliton generation in auxiliary-assisted microcavities *Light Sci. Appl.* **8** 50
[65] Stern B, Ji X, Okawachi Y, Gaeta A L and Lipson M 2018 Battery-operated integrated frequency comb generator *Nature* **562** 401–5
[66] Ferrera M, Razzari L, Duchesne D, Morandotti R, Yang Z, Liscidini M, Sipe J E, Chu S, Little B E and Moss D J 2008 Low-power continuous-wave nonlinear optics in doped silica glass integrated waveguide structures *Nat. Photon.* **2** 737–40
[67] Pasquazi P A, Park Y, Little B E, Chu S T, Moss D J and Morandotti R 2012 Demonstration of a stable ultrafast laser based on a nonlinear microcavity *Nat. Commun.* **3** 1–6
[68] Pasquazi A, Peccianti M, Little B E, Chu S T, Moss D J and Morandotti R 2012 Stable, dual mode, high repetition rate mode-locked laser based on a microring resonator *Opt. Exp.* **20** 27355–62
[69] Pasquazi A *et al* 2013 Self-locked optical parametric oscillation in a CMOS compatible microring resonator: a route to robust optical frequency comb generation on a chip *Opt. Exp.* **21** 13333–41
[70] Pasquzai A, Park Y, Azana J, Legare F, Morandotti R, Little B E, Chu S T and Moss D J 2010 Efficient wavelength conversion and net parametric gain via four wave mixing in a high index doped silica waveguide *Opt. Exp.* **18** 7634–41
[71] Peccianti M, Ferrera M, Razzari L, Morandotti R, Little B E, Chu S T and Moss D J 2010 Subpicosecond optical pulse compression via an integrated nonlinear chirper *Opt. Exp.* **18** 7625–33
[72] Duchesne D, Peccianti M, Lamont M R E, Ferrera M, Razzari L, Legare F, Morandotti R, Chu S, Little B E and Moss D J 2010 Supercontinuum generation in a high index doped silica glass spiral waveguide *Opt. Exp.* **18** 923–30
[73] Bao H, Olivieri L, Rowley M, Chu S T, Little B E, Morandotti R, Moss D J, Gongora J S T, Peccianti M and Pasquazi A 2020 Turing patterns in a fibre laser with a nested micro-resonator: robust and controllable micro-comb generation *Phys. Rev. Res.* **2** 023395
[74] Lauro L D, Li J, Moss D J, Morandotti R, Chu S T, Peccianti M and Pasquazi A 2017 Parametric control of thermal self-pulsation in micro-cavities *Opt. Lett.* **42** 3407–10
[75] Bao H, Cooper A, Chu S T, Moss D J, Morandotti R, Little B E, Peccianti M and Pasquazi A 2018 Type-II micro-comb generation in a filter-driven four wave mixing laser *Photonics Res.* **6** B67–B73
[76] Ferrera M, Park Y, Razzari L, Little B E, Chu S T, Morandotti R, Moss D J and Azaña J 2011 On-chip ultra-fast 1st and 2nd order CMOS compatible all-optical integration *Opt. Express* **19** 23153–61
[77] Wang W *et al* 2018 Robust soliton crystals in a thermally controlled microresonator *Opt. Lett.* **43** 2002–5
[78] Corcoran B *et al* 2020 Ultra-dense optical data transmission over standard fibre with a signal chip source *Nat. Commun.* **11** 2568
[79] Marin-Palomo P *et al* 2017 Microresonator-based solitons for massively parallel coherent optical communication *Nature* **546** 274
[80] Pfeifle J *et al* 2014 Coherent terabit communications with microresonator Kerr frequency combs *Nat. Photon.* **8** 375–80
[81] Xu X *et al* 2020 Photonic perceptron based on a Kerr microcomb for scalable high speed optical neural networks *Laser Photonics Rev.* **14** 2000070
[82] Xu X *et al* 2021 11 TOPS photonic convolutional accelerator for optical neural networks *Nature* **589** 44–51
[83] Feldmann J *et al* 2021 Parallel convolutional processing using an integrated photonic tensor core *Nature* **589** 52–58
[84] Reimer C *et al* 2015 Cross-polarized photon-pair generation and bi-chromatically pumped optical parametric oscillation on a chip *Nat. Commun.* **6** 8236
[85] Caspani L *et al* 2016 Multifrequency sources of quantum correlated photon pairs on-chip: a path toward integrated quantum frequency combs *Nanophotonics* **5** 351–62
[86] Reimer C *et al* 2016 Generation of multiphoton entangled quantum states by means of integrated frequency combs *Science* **351** 1176–80
[87] Kues M *et al* 2017 On-chip generation of high-dimensional entangled quantum states and their coherent control *Nature* **546** 622–6
[88] Roztocki P *et al* 2017 Practical system for the generation of pulsed quantum frequency combs *Opt. Express* **25** 18940–9
[89] Zhang Y *et al* 2020 Induced photon correlations through superposition of two four-wave mixing processes in integrated cavities *Laser Photonics Rev.* **14** 2000128
[90] Kues M, Reimer C, Lukens J M, Munro J, Weiner A M, Moss D J and Morandotti R 2019 Quantum optical micro-combs *Nat. Photon.* **13** 170–9
[91] Reimer C *et al* 2019 High-dimensional one-way quantum processing implemented on d-level cluster states *Nat. Phys.* **15** 148–53
[92] McClellan J, Parks T W and Rabiner L 1973 A computer program for designing optimum FIR linear phase digital filters *Trans. Audio Electroacoust.* **21** 506–26